Multicolor upconversion luminescence of $GdVO_4:Ln^{3+}/Yb^{3+}$ ($Ln^{3+} = Ho^{3+}$, Er^{3+}, Tm^{3+}, $Ho^{3+}/Er^{3+}/Tm^{3+}$) nanorods

Tamara V. Gavrilović [a], Dragana J. Jovanović [a], Krisjanis Smits [b], Miroslav D. Dramićanin [a, *]

[a] Vinča Institute of Nuclear Sciences, University of Belgrade, P.O. Box 522, 11001, Serbia
[b] Institute of Solid State Physics, University of Latvia, 19 Raina Blvd., Riga, Latvia

ABSTRACT

Lanthanide-doped $GdVO_4$ nanorods that exhibit upconversion emission under 982 nm excitation have been prepared by a facile room-temperature chemical co-precipitation method followed by a subsequent annealing at temperatures of 600 °C, 800 °C and 1000 °C. Multicolor upconversion emission, including white, was achieved by tuning the concentrations of dopant lanthanide ions (Ho^{3+}, Er^{3+}, Tm^{3+} and Yb^{3+}) in $GdVO_4$. It is found that four $GdVO_4$ samples emit light with the white chromaticity coordinates of (0.326, 0.339), (0.346, 0.343), (0.323, 0.327) and (0.342, 0.340) respectively, under a single-wavelength NIR excitation. These coordinates are very close to the standard equal energy white light coordinates (0.333, 0.333) according to the 1931 CIE diagram. By varying dopant lanthanide concentrations in nanorods it is possible to produce upconversion emission with colors between red (0.504, 0.369), green (0.282, 0.577) and blue (0.142, 0.125) coordinates.

© 2015 Elsevier Ltd. All rights reserved.

1. Introduction

Recent years have witnessed great interest in white light generation for a variety of applications, such as flat panel displays, three dimensional volumetric displays, solid-state lighting, liquid crystal back lights, light emitting diodes, and biomedical imaging [1–4]. In upconversion (UC) emission, which is a nonlinear multi-step optical process that yields a visible or near-infrared (NIR) emission through multiple absorption at NIR wavelengths, different colors of UC emission from one material can be achieved by doping the material with a different lanthanide ions [4–8]. In general, any emission color, including white, can be produced by mixing emissions of three primary colors, red (R), green (G) and blue (B). Therefore, an appropriate choice of dopant Ln^{3+} ions, like Er^{3+}, Ho^{3+}, Tm^{3+}, Pr^{3+} and Tb^{3+}, may create targeted a color of UC emission under a single-wavelength NIR excitation. For instance, red, green and blue UC emissions can be respectively obtained from the Ho^{3+}, Er^{3+}, and Tm^{3+}- doped materials, and UC emission of other colors by tuning the concentration ratio of these ions [9]. Additional doping of materials with Yb^{3+} ions, which have a large absorption cross-section at 982 nm and facilitate the stepwise

energy transfer to emitting ions, increases the UC emission intensity by several orders of magnitude compared to the systems without Yb^{3+} ions. Although there is a large number of literature reports on multicolor and white light production by down-conversion emission of lanthanides, the UC still has to be extensively researched [1–3,9–16].

In particular, the study of lanthanide doped nanomaterials for multicolor UC applications, in both fundamental science and technological research, is important since UC nanoparticles are promising alternatives to traditional phosphors due to the reduced light scattering and potential applications in biomedicine.

Herein, the goal was to prepare and optically characterize nanocrystalline powders of Ln^{3+} doped $GdVO_4$ that show tunable multicolor UC emission under single-wavelength excitation at 982 nm. For this reason Ho^{3+}, Er^{3+}, Tm^{3+}, and Yb^{3+}- doped $GdVO_4$ nanorods were prepared by a room-temperature chemical co-precipitation method and subsequent annealing route. Tetragonal zircon-type gadolinium orthovanadate is a well-established host for lanthanide ions with good features such as moderate cut-off phonon energy and relatively high thermal conductivity [14]. Because of the same charges and similar ionic radii, electronic structures and electronegativities, through doping of $GdVO_4$, over a wide range of doping concentrations, a part of Gd^{3+} ions can be easily substituted by other Ln^{3+} ions without causing much change

---

in the lattice structure [17]. We examined UC emission properties of $GdVO_4$ nanorods doped with different concentrations of lanthanide ions, and calculated the color chromaticity coordinates of obtained emissions.

2. Experimental details

2.1. Synthesis of $GdVO_4$:Ln^{3+}/Yb^{3+} ($Ln^{3+} = Er^{3+}$, Ho^{3+}, Tm^{3+}, Tm^{3+}/Ho^{3+}/Er^{3+})

A chemical co-precipitation technique was used to prepare $GdVO_4$:Ln^{3+}/Yb^{3+} ($Ln^{3+} = Er^{3+}$, Ho^{3+}, Tm^{3+}, Tm^{3+}/Ho^{3+}/Er^{3+}) with different Ln^{3+}/Yb^{3+} concentration ratio, such as: $Gd_{1-x-w}Tm_xYb_wVO_4$ (x = 0.03; w = 0.1), $Gd_{1-y-w}Er_yYb_wVO_4$ (y = 0.02; w = 0.1), $Gd_{1-z-w}Ho_zYb_wVO_4$ (z = 0.01; w = 0.1) and $Gd_{1-x-y-z-w}Tm_xEr_yHo_zYb_wVO_4$ (x = 0.03, 0.1; y = 0.01, 0.02; z = 0.005, 0.01; w = 0.1, 0.2, 0.4).

All chemicals: gadolinium(III)-nitrate hexahydrate, $Gd(NO_3)_3 \times 6H_2O$ (99.9%, Alfa Aesar), erbium(III)-nitrate pentahydrate, $Er(NO_3)_3 \times 5H_2O$ (99.9%, Alfa Aesar), holmium(III)-nitrate pentahydrate, $Ho(NO_3)_3 \times 5H_2O$ (99.9%, Alfa Aesar), thulium(III)-nitrate pentahydrate, $Tm(NO_3)_3 \times 5H_2O$ (99.9%, Alfa Aesar), ytterbium(III)-nitrate pentahydrate, $Yb(NO_3)_3 \times 5H_2O$ (99.9%, Alfa Aesar), amonium-vanadium oxide, NH_4VO_3 (min. 99.0%, Alfa Aesar) and sodium-hydroxide, NaOH (min. 99%, Moss Hemos) were of the highest purity available and were used without any further purification.

An appropriate amount of NH_4VO_3 was dissolved into a (aq) 0.15 M NaOH resulting in a 0.05 M Na_3VO_4 with a pH = 12. The mixture of 0.05 M aqueous solutions of Gd^{3+} ions and Ln^{3+}/Yb^{3+} ions in the corresponding stoichiometric ratio was afterwards added drop wise (1drop/3sec) in a Na_3VO_4 solution. A formed milk-white opalescent precipitate of $Gd_{1-x-y-z-w}Tm_xEr_yHo_zYb_wVO_4$ and mixture was additionally heated and stirred at 60 °C for 1 h. The pH value of a milk-white suspension was about 9. In order to adjust the pH value to 7, the precipitate was then separated from the suspension by centrifugation, and washed out several times with distilled water. Finally, the powders of $Gd_{1-x-y-z-w}Tm_xEr_yHo_zYb_wVO_4$, were collected and dried at 60 °C in air for 20 h.

The dried materials, which were synthesized with different combinations of dopant ions (Ho^{3+}/Yb^{3+}, Er^{3+}/Yb^{3+}, Tm^{3+}/Yb^{3+}, Ho^{3+}/Er^{3+}/Tm^{3+}/Yb^{3+}), are referred to as "as-prepared" samples. To further enhance their crystallinity, the as-prepared samples in Series 1, Series 2 and Series 3 (see Table 1) were additionally annealed at different temperatures T_a (300 °C, 600 °C, 800 °C and 1000 °C) for 2 h. Similarly, the as-prepared samples in Series 4 and Series 5 (Table 1) were heat-treated at 800 °C and at 1000 °C for 2 h. As shown in Table 1, a total of 36 samples, divided in 5 groups, were prepared.

2.2. Instruments

Powder X-ray diffraction (XRD) measurements were performed on a Rigaku SmartLab diffractometer using Cu-Kα radiation (λ = 0.15405 nm). Diffraction data were recorded with a step size of 0.02° and a counting time of 0.7° min^{-1} over the angular range of 10° ≤ 2θ ≤ 100°. Crystallite sizes were estimated using the Halder–Wagner method by analyzing all major diffraction peaks.

Transmission electron microscopy (TEM) studies were made on a Tecnai G20 (FEI) operated at an accelerating voltage of 200 kV. Samples were supported on a perforated carbon film (S147-4, Agar scientific) and were dried in air for one day. It was observed that at a high electron radiation dose defects were induced into the crystals until their crystal structure disappeared. Therefore, for HRTEM images the electron beam intensity was reduced strongly by

inserting a condenser aperture and by decreasing the spot size. TEM micrographs showed that the powders in Series 4 and Series 5 (Table 1) had relatively large grains, therefore scanning electron microscopy (SEM) measurements were also performed. SEM studies were made on a SEM Lyra (Tescan) operated at 25 kV. Samples were placed on a carbon adhesive tape and coated with gold.

All room temperature UC luminescence emission spectra were measured under 982 nm (MDLH 980 3w diode laser with controller) excitation and detected with an AvaSpec-2048 Fiber Optic Spectrometer system.

3. Results and discussion

3.1. Structural and morphological characterization

The phase identity and purity of all of the prepared powders were investigated by XRD. All samples were nanocrystalline with zircon-type crystal structure. XRD patterns of Ho^{3+}/Yb^{3+} co-doped $GdVO_4$ of as-prepared and annealed samples are given in Fig. 1 as representative examples. All patterns clearly showed the presence of single tetragonal zircon-type $GdVO_4$ crystal structure with space group $I4_1$/amd (JCPDS card no. 17-0260). No traces of any impurity phases were noticed indicating that the dopant ions were successfully incorporated into the host lattice. Clearly, the full width at half maximum of diffraction peaks was gradually narrowed as the annealing temperature increased up to 1000 °C.

The structural parameters of the 1Ho10Yb-samples were evaluated by Rietveld refinement of the XRD data and results of the analysis are summarized in Table 2. Microstrain values are low suggesting good ion ordering in the nanocrystals. The average crystallite size calculated by the Halder–Wagner method changes from 14 nm to 59 nm for the as-prepared sample and the sample annealed at 1000 °C, respectively. The Rietveld R-factors, profile factor (Rp), weighted profile factor (Rwp) and the expected-weighted profile factor (Re), as well as the goodness of fit (GOF) are small indicating a highly satisfactory reliability of the fitting procedure.

In general, the crystallinity of the nanoparticles can be improved when samples are additionally heat-treated. As shown by morphological and structural analysis, the Ln^{3+}-doping did not change the crystal structure and morphology of the synthesized materials. All prepared samples were nanocrystalline and had similar morphology of particles − nanorods; typical TEM and SEM images, obtained for Ho^{3+}/Yb^{3+} co-doped $GdVO_4$ samples, are shown in Fig. 2. Low magnification TEM images for 1Ho10Yb-ap and 1Ho10Yb-300 samples (Fig. 2(a) and (b)) suggest that powders are self-organized in bundles of nanorods aligned at different orientations, while high magnification (Fig. 2(b) and (d)) suggest that the bundles contain 5-6 individual nanorods (up to 20 nm in length and from 5 nm in diameter). Images of samples annealed at a temperature of 600 °C show that the nanorods grow into single ellipsoidal particles (about 20 nm in size) (Fig. 2(e) and (f)). The powders annealed at 800 °C and 1000 °C had larger grains, and their morphology was observed by SEM (Fig. 2(g) and (h)); the micrographs suggest that powder 1Ho10Yb-800 contains non-regular spheres with size about 100 nm, while 1Ho10Yb-1000 powder contains long rods with diameter of about 1−2 μm.

3.2. Upconverting (UC) luminescence in $GdVO_4$:Ln^{3+}/Yb^{3+} samples

The UC luminescence of all annealed $GdVO_4$:Ln^{3+}/Yb^{3+} ($Ln^{3+} = Ho^{3+}$, Er^{3+}, Tm^{3+} and Ho^{3+}/Er^{3+} Tm^{3+}) samples (see Table 1 for compositions) can be clearly observed under the excitation of a 982 nm laser diode. The influence of a post-synthesis

Table 1
Sample names and abbreviated sample names (with dopant ions type and doping concentrations) of all prepared $GdVO_4$:Ln^{3+}/Yb^{3+} ($Ln^{3+} = Er^{3+}$, Ho^{3+}, Tm^{3+}, Tm^{3+}/Ho^{3+}/Er^{3+}) powders, as-prepared (ap) and heat-treated at different temperatures (300, 600, 800, 1000 °C).

Sample number	Sample names	Abbreviated sample names
Series 1		
S11	$Gd_{0.89}Ho_{0.01}Yb_{0.1}VO_4$-ap	1Ho10Yb-ap
S12	$Gd_{0.89}Ho_{0.01}Yb_{0.1}VO_4$-300C	1Ho10Yb-300
S13	$Gd_{0.89}Ho_{0.01}Yb_{0.1}VO_4$-600C	1Ho10Yb-600
S14	$Gd_{0.89}Ho_{0.01}Yb_{0.1}VO_4$-800C	1Ho10Yb-800
S15	$Gd_{0.89}Ho_{0.01}Yb_{0.1}VO_4$-1000C	1Ho10Yb-1000
Series 2		
S21	$Gd_{0.88}Er_{0.02}Yb_{0.1}VO_4$-ap	2Er10Yb-ap
S22	$Gd_{0.88}Er_{0.02}Yb_{0.1}VO_4$-300C	2Er10Yb-300
S23	$Gd_{0.88}Er_{0.02}Yb_{0.1}VO_4$-600C	2Er10Yb-600
S24	$Gd_{0.88}Er_{0.02}Yb_{0.1}VO_4$-800C	2Er10Yb-800
S25	$Gd_{0.88}Er_{0.02}Yb_{0.1}VO_4$-1000C	2Er10Yb-1000
Series 3		
S31	$Gd_{0.87}Tm_{0.03}Yb_{0.1}VO_4$-ap	3Tm10 Yb-ap
S32	$Gd_{0.87}Tm_{0.03}Yb_{0.1}VO_4$-300C	3Tm10Yb-300
S33	$Gd_{0.87}Tm_{0.03}Yb_{0.1}VO_4$-600C	3Tm10Yb-600
S34	$Gd_{0.87}Tm_{0.03}Yb_{0.1}VO_4$-800C	3Tm10Yb-800
S35	$Gd_{0.87}Tm_{0.03}Yb_{0.1}VO_4$-1000C	3Tm10Yb-1000
Series 4		
S41	$Gd_{0.84}Tm_{0.03}Er_{0.02}Ho_{0.01}Yb_{0.1}VO_4$-ap	3Tm2Er1Ho10Yb-ap
S42	$Gd_{0.84}Tm_{0.03}Er_{0.02}Ho_{0.01}Yb_{0.1}VO_4$-800C	3Tm2Er1Ho10Yb-800
S43	$Gd_{0.84}Tm_{0.03}Er_{0.02}Ho_{0.01}Yb_{0.1}VO_4$-1000C	3Tm2Er1Ho10Yb-1000
S44	$Gd_{0.74}Tm_{0.03}Er_{0.02}Ho_{0.01}Yb_{0.2}VO_4$-ap	3Tm2Er1Ho20 Yb-ap
S45	$Gd_{0.74}Tm_{0.03}Er_{0.02}Ho_{0.01}Yb_{0.2}VO_4$-800C	3Tm2Er1Ho20 Yb-800
S46	$Gd_{0.74}Tm_{0.03}Er_{0.02}Ho_{0.01}Yb_{0.2}VO_4$-1000C	3Tm2Er1Ho20 Yb-1000
S47	$Gd_{0.54}Tm_{0.03}Er_{0.02}Ho_{0.01}Yb_{0.4}VO_4$-ap	3Tm2Er1Ho40 Yb-ap
S48	$Gd_{0.54}Tm_{0.03}Er_{0.02}Ho_{0.01}Yb_{0.4}VO_4$-800C	3Tm2Er1Ho40 Yb-800
S49	$Gd_{0.54}Tm_{0.03}Er_{0.02}Ho_{0.01}Yb_{0.4}VO_4$-1000C	3Tm2Er1Ho40 Yb-1000
Series 5		
S51	$Gd_{0.475}Tm_{0.1}Er_{0.02}Ho_{0.005}Yb_{0.4}VO_4$-ap	10Tm2Er0.5Ho40 Yb-ap
S52	$Gd_{0.475}Tm_{0.1}Er_{0.02}Ho_{0.005}Yb_{0.4}VO_4$-800C	10Tm2Er0.5Ho40 Yb-800
S53	$Gd_{0.475}Tm_{0.1}Er_{0.02}Ho_{0.005}Yb_{0.4}VO_4$-1000C	10Tm2Er0.5Ho40 Yb-1000
S54	$Gd_{0.47}Tm_{0.1}Er_{0.02}Ho_{0.01}Yb_{0.4}VO_4$-ap	10Tm2Er1Ho40 Yb-ap
S55	$Gd_{0.47}Tm_{0.1}Er_{0.02}Ho_{0.01}Yb_{0.4}VO_4$-800C	10Tm2Er1Ho40 Yb-800
S56	$Gd_{0.47}Tm_{0.1}Er_{0.02}Ho_{0.01}Yb_{0.4}VO_4$-1000C	10Tm2Er1Ho40 Yb-1000
S57	$Gd_{0.555}Tm_{0.03}Er_{0.01}Ho_{0.005}Yb_{0.4}VO_4$-ap	3Tm1Er0.5Ho40 Yb-ap
S58	$Gd_{0.555}Tm_{0.03}Er_{0.01}Ho_{0.005}Yb_{0.4}VO_4$-800C	3Tm1Er0.5Ho40 Yb-800
S59	$Gd_{0.555}Tm_{0.03}Er_{0.01}Ho_{0.005}Yb_{0.4}VO_4$-1000C	3Tm1Er0.5Ho40 Yb-1000
S510	$Gd_{0.545}Tm_{0.03}Er_{0.02}Ho_{0.005}Yb_{0.4}VO_4$-ap	3Tm2Er0.5Ho40 Yb-ap
S511	$Gd_{0.545}Tm_{0.03}Er_{0.02}Ho_{0.005}Yb_{0.4}VO_4$-800C	3Tm2Er0.5Ho40 Yb-800
S512	$Gd_{0.545}Tm_{0.03}Er_{0.02}Ho_{0.005}Yb_{0.4}VO_4$-1000C	3Tm2Er0.5Ho40 Yb-1000
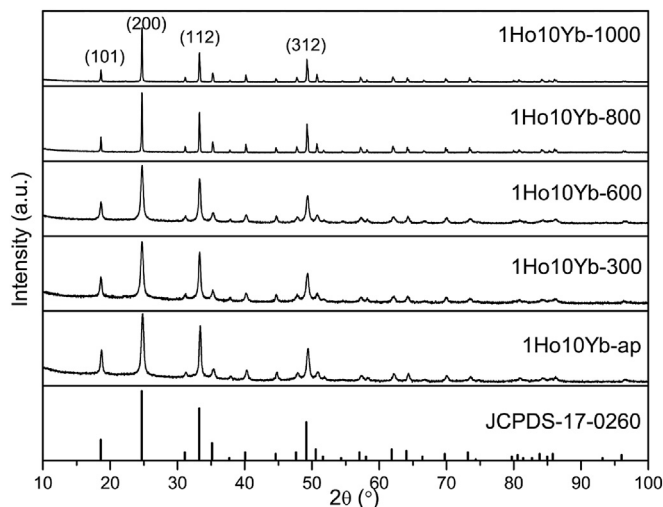
Fig. 1. Room temperature XRD patterns for $Gd_{0.89}Ho_{0.01}Yb_{0.1}VO_4$ samples, as-prepared and annealed at different temperatures (Series 1 in Table 1). Vertical bars denote the standard data for a tetrahedral zircon structure of a bulk $GdVO_4$ (JCPDS, card No. 17-0260).

thermal treatment was noticed in all recorded spectra. It was found that there is an increase in the intensity of the UC emission peaks with the increase of annealing temperature, with maximal emission intensity found for samples annealed at 1000 °C. This enhancement of UC emission is a consequence of the higher crystallinity and larger size of particles obtained at high temperatures, as well as the more-efficient removal of adsorbed species on the surface of particles at elevated temperatures. For this reason, UC emission properties of the samples prepared at 800 °C and 1000 °C are further considered and analyzed.

3.2.1. Red, green and blue UC emissions

The room-temperature UC spectra of $GdVO_4$:Ln^{3+}/Yb^{3+} ($Ln^{3+} = Er^{3+}$, Ho^{3+}, Tm^{3+}) samples prepared at 800 °C and 1000 °C are depicted in Fig. 3.

An analysis of these spectra was facilitated by schematic energy level diagrams of Yb^{3+}, Ho^{3+}, Er^{3+}, and Tm^{3+} ions presented in Fig. 4. Three combinations of dopants in $GdVO_4$, Ho^{3+}/Yb^{3+}, Er^{3+}/Yb^{3+} and Tm^{3+}/Yb^{3+}, gave (under the 982 nm irradiation), respectively, red, green and blue (in web version) UC emission which was directly visible by eye.

Ho^{3+}/Yb^{3+} co-doped $GdVO_4$ samples exhibit two emission bands in their UC luminescence spectra: weak green emission centered at 542 nm can be assigned to transitions from $^5F_4$ and $^5S_2$

Table 2
Structural details of synthesized $Gd_{0.89}Ho_{0.01}Yb_{0.1}VO_4$ samples, as-prepared and heat-treated at different temperatures (Series 1 in Table 1), calculated using Rietveld refinement.

	1Ho10Yb-ap	1Ho10Yb-300	1Ho10Yb-600	1Ho10Yb-800	1Ho10Yb-1000
a = b	7.1921(7)	7.1866(7)	7.1821(13)	7.1903(3)	7.1899(4)
c	6.3379(6)	6.3334(6)	6.3281(12)	6.3362(3)	6.3360(4)
Crystallite size (nm)	14.7(2)	16.2(3)	17.2(6)	52.6(6)	59.0(3)
Strain	0.23(10)	0.28(9)	0.16(2)	0.06(4)	0.033(13)
Rwp (%)	3.34	3.40	2.69	3.71	4.32
Rp (%)	2.56	2.58	2.06	2.71	3.20
Re (%)	2.18	2.14	2.19	2.44	2.33
GOF	1.5312	1.5884	1.2292	1.5228	1.8515

levels to the $^5I_8$ ground level of Ho^{3+}, while an intense red emission, centered at 659 nm, is due to the $^5F_5 \rightarrow {}^5I_8$ transition (see Fig. 3(A)). The calculated CIE chromaticity coordinates of 1Ho10Yb-1000 (S15) and 1Ho10Yb-800 (S14) samples are (x = 0.504, y = 0.369) and (x = 0.411, y = 0.362), respectively, and they are located in the red and orange spectral regions. The red to green emission ratio of 1Ho10Yb-1000 is larger than the ratio of 1Ho10Yb-800.

It is interesting to note, that, unlike the majority of phosphors, Ho^{3+}/Yb^{3+}-co-doped $GdVO_4$ exhibits both strong green down-conversion emission and strong red UC emission [20]. A predominantly green UC emission is frequently observed in Ho^{3+}/Yb^{3+}-co-doped inorganic materials, while dominant red UC emission has been rarely reported [18]. Moreover, the strong red UC emission is usually reported for relatively high concentrations of Ho^{3+} and explained by cross-relaxations among different levels of Ho^{3+} which inhibits green UC emission [19,20]. However, in this study, we find strong red UC emission for relatively small Ho^{3+} concentrations, and for all Ho^{3+}/Yb^{3+} concentration ratios (for more details on this phenomenon see Ref. 20 and references therein).

The UC emission spectra of $GdVO_4$:Er^{3+}/Yb^{3+} powders consist of two strong peaks in the green spectral range, at 525 nm (from $^2H_{11/2} \rightarrow {}^4I_{15/2}$ transition) and at 552 nm (from $^4S_{3/2} \rightarrow {}^4I_{15/2}$ transition), and a weak peak centered around 655 nm (from $^4F_{9/2} \rightarrow {}^4I_{15/2}$ transition) (see Fig. 3 (B) and 4). All these emissions are generated by Er^{3+} ions after being directly excited and excited via $Yb^{3+} \rightarrow Er^{3+}$ energy transfers. In these samples, the green UC emission is more intense than the red one, and the green/red intensity ratio increases with increasing sample preparation temperature. The calculated CIE 1931 chromaticity coordinates are (0.282, 0.577) and (0.290, 0.446), respectively, for 2Er10Yb-1000 (S25) and 2Er10Yb-800 (S24), and are in the green and green-yellow color space regions.

The $GdVO_4$:Tm^{3+}/Yb^{3+} samples exhibit UC spectra with three distinct bands in a blue, red and near-infrared spectral regions which can be assigned to 4f-4f transitions of $^1G_4 \rightarrow {}^3H_6$ (475 nm), $^1G_4 \rightarrow {}^3F_4$ (650 nm) and $^3H_4 \rightarrow {}^3H_6$ (800 nm), respectively (see Fig. 3 (C) and 4). Two emissions are strong, at 475 nm and at 800 nm, while the emission at 650 nm is very weak. The calculated chromaticity coordinates (x, y) of 3Tm10Yb-1000 (S35) and 3Tm10Yb-800 (S34) are (0.142, 0.125) and (0.14288, 0.12451) respectively, which are located in the blue color region.

On the basis of energy-matching conditions, the possible mechanisms for population of emitting levels, as well as radiative and non-radiative pathways are illustrated in Fig. 4 [9,11,13,14]. Following an 982 nm excitation, an excited Yb^{3+} ion transfers its energy to Ho^{3+} ion in the $^5I_8$ ground state, which results in an excitation of Ho^{3+} to the relatively long-lived excited state $^5I_6$. For a green emission, first, Ho^{3+} ions in the $^5I_6$ state accept energy from the excited Yb^{3+} and transfer to the $^5F_4/^5S_2$ levels, and then to the $^5I_8$ level, producing a green emission band centered at 542 nm. For a red emission, first, Ho^{3+} ions in the $^5I_6$ level de-excite to the lower-

energy $^5I_7$ level via a nonradiative phonon-assisted relaxation; then, upon receiving energy from the excited Yb^{3+} ions, the higher $^5F_5$ level is populated. Finally, the radiative transfer from $^5F_5$ ions to the ground state $^5I_8$ results in a red emission centered at 650 nm. Clearly, the levels $^5F_4/^5S_2$ and $^5F_5$ of Ho^{3+} can be populated by two successive energy transfers from excited Yb^{3+} [21].

The energy of the $^4I_{11/2}$ level of Er^{3+} is very similar to that of the $^2F_{5/2}$ level of Yb^{3+}; thus, both Er^{3+} and Yb^{3+} absorb 982-nm photons. However, the absorption cross-section of the $^2F_{7/2} \rightarrow {}^2F_{5/2}$ transition of Yb^{3+} is much larger than that of the $^4I_{15/2} \rightarrow {}^4I_{11/2}$ transition of Er^{3+} and the Yb^{3+} ions absorb most of the excitation energy, therefore, the energy levels of Er^{3+} are mainly populated by the energy transfers from the excited Yb^{3+} ions. Following an absorption of a 982 nm photon, an excited Yb^{3+} ion transfers its excitation energy to the $^4I_{11/2}$ Er^{3+} level. For green emissions, first, a second energy transfer from another excited Yb^{3+} to a previously excited Er^{3+} ion leads to the excitation of the Er^{3+} ion from the $^4I_{11/2}$ to the upper $^4I_{7/2}$ level. Next, nonradiative phonon-assisted relaxations occurs between $^4I_{7/2}$ excited level and $^2H_{11/2}$, $^4S_{3/2}$ emissions levels. For a red emission, first, the de-excitation of Er^{3+} ions in the $^4I_{11/2}$ level via a nonradiative phonon-assisted relaxation leads to the lower $^4I_{13/2}$ level; then, upon receiving energy from the excited Yb^{3+} ions, the Er^{3+} ions transit to the higher $^4I_{9/2}$ level. The radiative relaxation of these higher energy states produces UC emission. The two green bands at 525 and 552 nm are realized in the cases of relaxation from excited-state levels $^2H_{11/2}$ and $^4S_{3/2}$ to the Er^{3+} ground state ($^4I_{15/2}$), while very weak red emission at 660 nm corresponding to relaxation from the excited-state level $^4F_{9/2}$ to the Er^{3+} ground state. The overall UC process requires the absorption of two photons in each case [22].

The blue and weak red and NIR emissions of Tm^{3+} can be obtained from the transitions of $^1G_4 \rightarrow {}^3H_6$, $^1G_4 \rightarrow {}^3F_4$ and $^3H_4 \rightarrow {}^3H_6$, respectively. The population of $^1G_4$ Tm^{3+} level can be explained by sequential three-photon energy transfer processes from excited $^2F_{5/2}$ Yb^{3+}, which in a first step populates $^3F_4$ level by multiphonon relaxation from the phonon-assisted excited $^3H_5$ state, then a second electronic energy transfer excites Tm^{3+} to $^3F_2$ level, which relaxes populating the infrared emitting $^3F_3$ and $^3H_4$ levels, and finally the third electronic energy transfer populates $^1G_4$ level which relaxes to the Tm^{3+} ground state ($^3H_6$) emitting blue emission at 475 nm and to the $^3F_4$ level emitting red emission at ~650 nm. The population of $^3H_4$ level is strongly favored by both relaxation from $^3F_2$ level and non-radiative decay after the second transfer from $^2F_{5/2}$ level of Yb^{3+} ions. The populated $^3H_4$ level relaxes to the ground state ($^3H_6$) giving a strong infrared emission at 800 nm [9,14].

3.2.2. Multicolor and white light UC luminescence

As discussed earlier, NIR-to-red, NIR-to-green, and NIR-to-blue upconversion luminescence was observed in Ho^{3+}/Yb^{3+}, Er^{3+}/Yb^{3+} and Tm^{3+}/Yb^{3+}-co-doped $GdVO_4$. Combinations of different
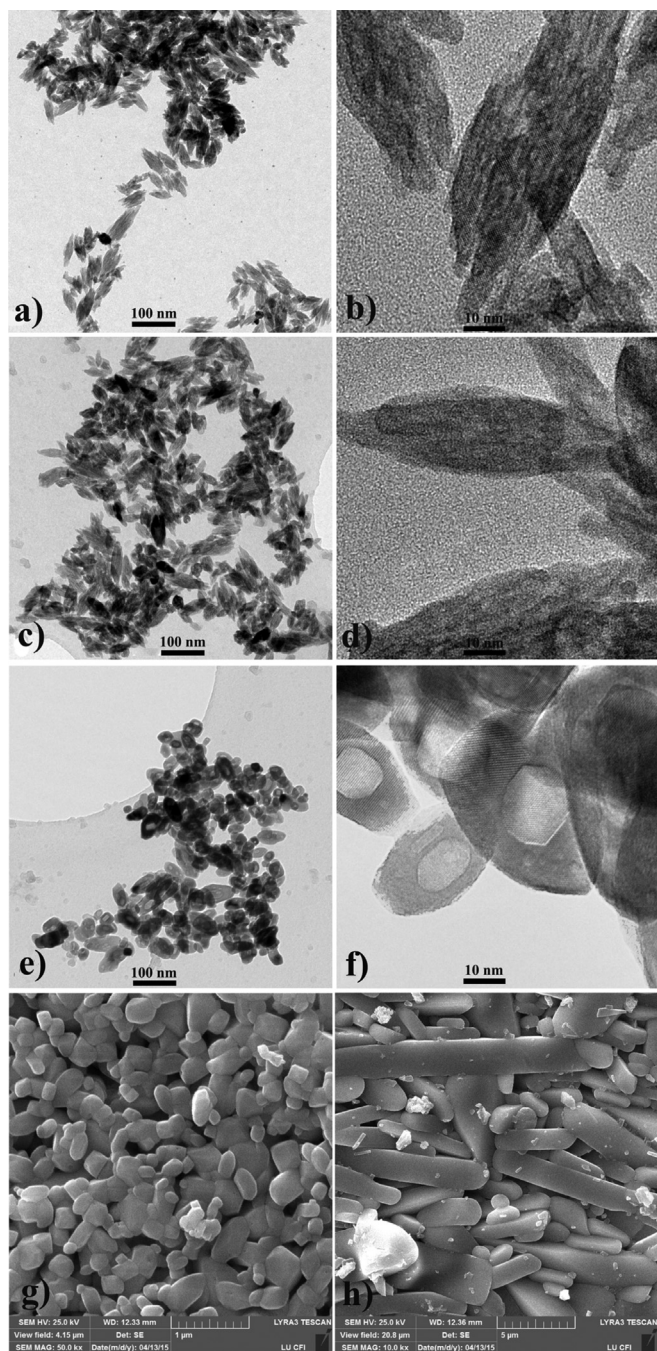
Fig. 2. TEM and SEM images of $Gd_{0.89}Ho_{0.01}Yb_{0.1}VO_4$ powders (Series 1 in Table 1). Low magnification (left-hand side) and high-resolution (right-hand side) TEM micrographs of the: (a, b) as-prepared sample; (c, d) the sample annealed at 300 °C and (e, f) the sample annealed at 600 °C. SEM images of the samples: (g) annealed at 800 °C (scale bar 1 μm) and (h) annealed at 1000 °C (scale bar 5 μm).

intensities of red, green and blue UC emission can produce light of different colors in the visible spectrum (including white). Additional $Ho^{3+}/Er^{3+}/Tm^{3+}$- doped and Yb^{3+}- co-doped $GdVO_4$ powder samples were prepared to further study multicolor (red, green, blue) luminescence of these materials under single wavelength excitation at 982 nm, and, in particular, to investigate the possibility of generating white light. First, samples having three different concentrations of Yb^{3+} (10, 20 and 40 mol%) and the constant concentrations of Ho^{3+} (1 mol%), Er^{3+} (2 mol%) and Tm^{3+} (3 mol%) were prepared at 800° and 1000 °C. (Series 4 in Table 1) and
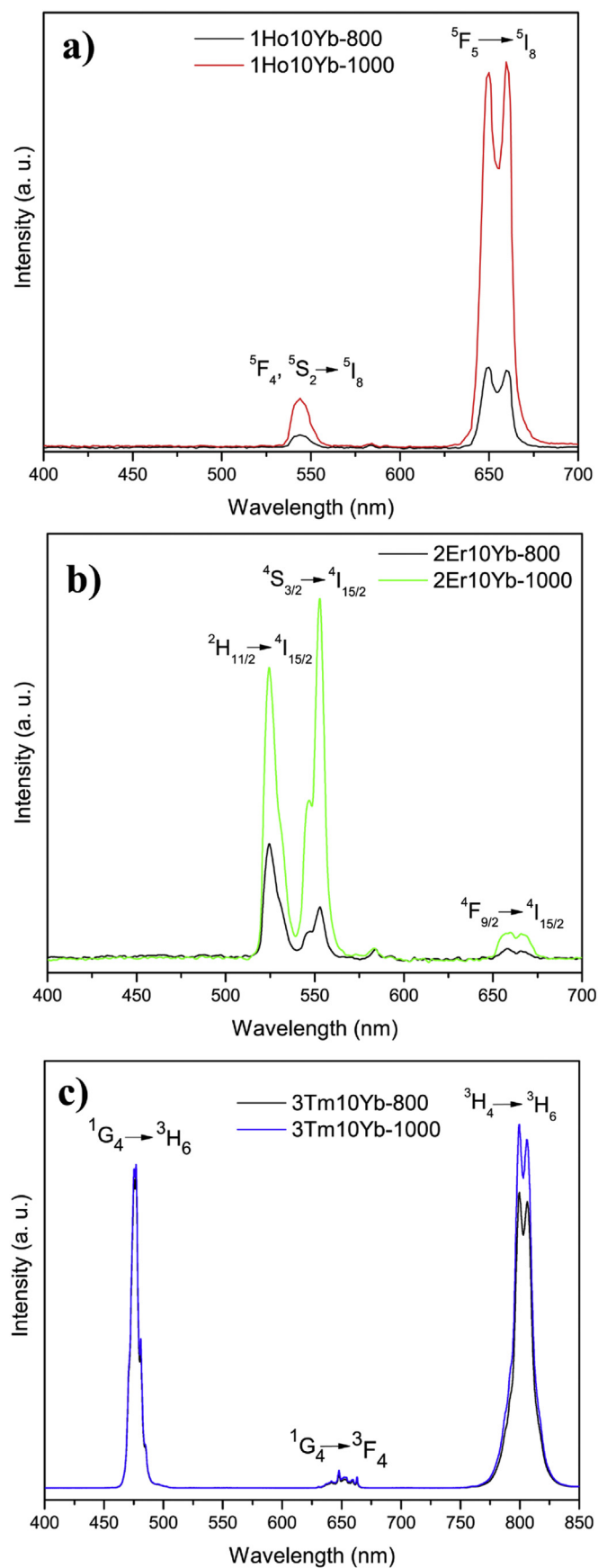
Fig. 3. Room-temperature UC emission spectra (under 980 nm excitation) of (a) Ho^{3+}/Yb^{3+}-, (b) Er^{3+}/Yb^{3+}- and (c) Tm^{3+}/Yb^{3+}-co-doped $GdVO_4$ powders annealed at 800 °C and 1000 °C. Abbreviated sample names are explained in Table 1.
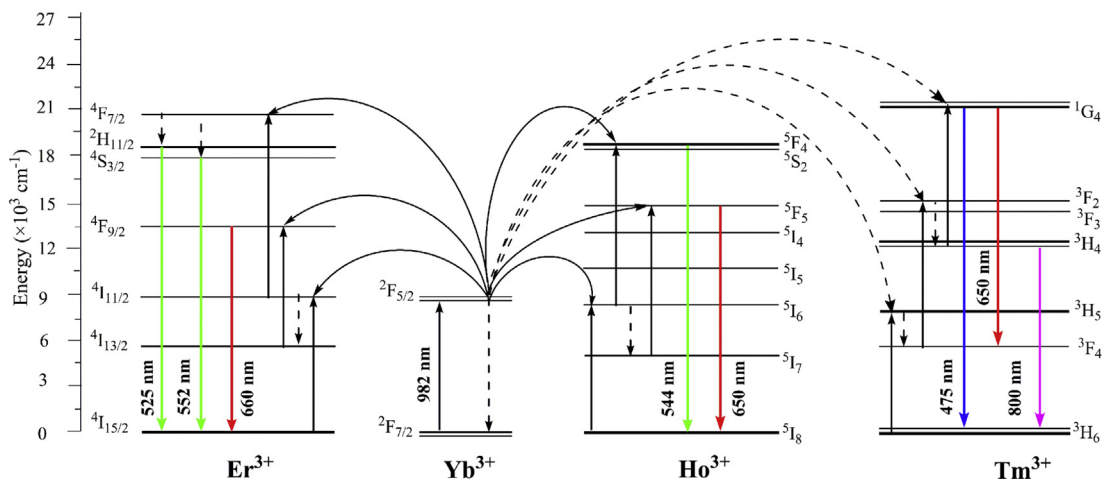
Fig. 4. Schematic energy level diagrams of Yb^{3+}, Er^{3+}, Ho^{3+} and Tm^{3+} and proposed UC mechanisms in the $Gd_{1-x-y-z-w}Tm_xEr_yHo_zYb_wVO_4$ nanorods.

analyzed. Then, samples were prepared (Series 5, Table 1) with constant concentration of Yb^{3+} (40 mol%) and having variable concentration of Ho^{3+}, Er^{3+} and Tm^{3+}, also at 800° and at 1000 °C.

Fig. 5 presents the UC luminescence spectra of white light for 10Tm2Er0.5Ho40Yb-800 sample excited with a 982 nm laser. It could be expected, therefore, that the $GdVO_4$:Ho^{3+}/Er^{3+}/Tm^{3+}/Yb^{3+} nanocrystalline powders would be tricolor (red-green-blue) emitting phosphors. However, it should be emphasized that, although the main UC processes of Ln^{3+} ions are well known, the relative intensities of the transitions influencing the color of the emission in the nanocrystalline $GdVO_4$:Ln^{3+}/Yb^{3+} depend non-linearly on the Ln^{3+} and Yb^{3+} concentrations and on non-radiative processes related to the host and its properties.

All 3Tm2Er1Ho10Yb-samples showed a strong red emission and about as half as strong green emission, while their blue emission was very weak. This finding is consistent with yellow luminescence of 3Tm2Er1Ho40Yb-1000 (S43) (see Table 3). To balance intensities of red, green, and blue emissions, Yb^{3+} concentration was increased in $GdVO_4$:Ho^{3+}/Er^{3+}/Tm^{3+}/Yb^{3+} samples (keeping the concentration ratio between Ho^{3+}, Er^{3+} and Tm^{3+} constant, Series 4 in Table 1). As a consequence, relative emission intensities were changed since the red and green emission intensities simultaneously decreased. The effect can be explained as follows: when the concentration of Yb^{3+} ions increases to reach the heavy doping level, the concentration quenching effect dominates the UC emission and leads to the decrease of both green and red emission bands of Ho^{3+} and Er^{3+} [23]. Emission color tuning in such a way, by varying the doping concentration of Yb^{3+}, resulted in one sample (with 40 mol% of Yb^{3+}) showing yellowish-white luminescence.

Yellowish-white luminescence of the 3Tm2Er1Ho40Yb-800 (S48) sample led us to synthesize and study a series of samples with constant Yb^{3+} concentration (40 mol%) and different concentration of Ho^{3+}, Er^{3+} and Tm^{3+} ions (Series 5 in Table 1). Experimentation with the samples of Series 4 also showed that, in order to obtain white-light emission, the intensity of blue light had to be further increased by increasing the doping concentration of Tm^{3+}. The observed UC emissions of multicolor and white light were converted to the CIE chromaticity coordinates which are listed in Table 3 and plotted in Fig. 6.
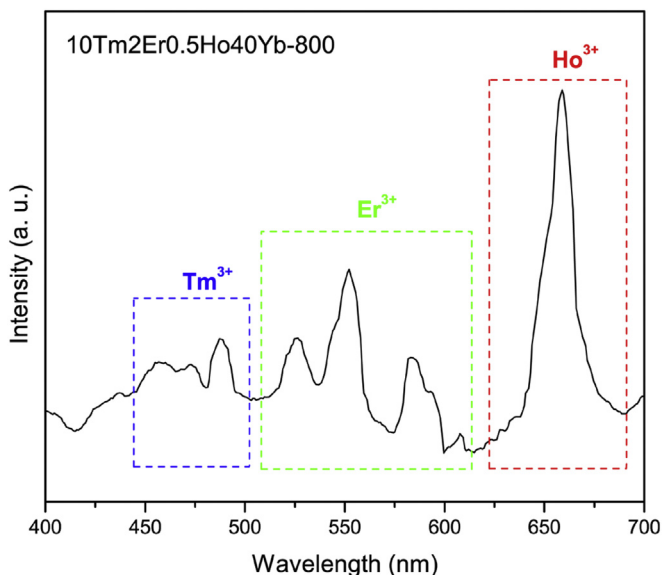
Fig. 5. UC emission spectra of white light for 10Tm2Er0.5Ho40 Yb-800 sample excited with a 982 nm laser.

Table 3
Calculated chromaticity coordinates (x, y) and emission color for prepared powders. Sample number are explained in Table 1.

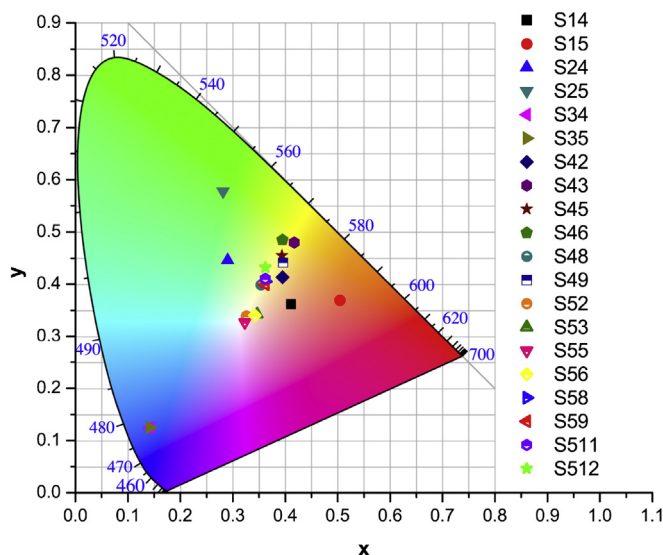| Sample number	Chromaticity coordinates (x, y)	Emission color
S14	(0.411, 0.362)	Orange
S15	(0.504, 0.369)	Red
S24	(0.290, 0.446)	Green-yellowish
S25	(0.282, 0.577)	Green
S34	(0.143, 0.124)	Blue
S35	(0.142, 0.125)	Blue
S42	(0.395, 0.413)	Orange
S43	(0.417, 0.480)	Yellow
S45	(0.394, 0.455)	Yellow
S46	(0.395, 0.485)	Yellow
S48	(0.354, 0.399)	Yellowish
S49	(0.396, 0.441)	Yellow−orange
S52	(0.326, 0.339)	White
S53	(0.346, 0.343)	White
S55	(0.323, 0.327)	White
S56	(0.342, 0.340)	White
S58	(0.362, 0.405)	Yellowish-white
S59	(0.407, 0.399)	Yellowish-white
S511	(0.354, 0.410)	Yellowish-white
S512	(0.408, 0.432)	Yellowish-white

Fig. 6. The CIE 1931 chromaticity diagram of $Gd_{1-x-y-z-w}Tm_xEr_yHo_zYb_wVO_4$ powders excited with a 982 nm laser.

A pure white light was obtained in four samples (S52, S53, S55, S56): the calculated chromaticity coordinates (x, y) of are (0.326, 0.339), (0.346, 0.343), (0.323, 0.327) and (0.342, 0.340), respectively. These coordinates fall in the white region and are very close to the standard equal energy white light coordinates (0.333, 0.333) according to the 1931 CIE diagram. Note that, so far, only several other UC white-emitting $Ho^{3+}/Er^{3+}/Tm^{3+}$- doped and Yb^{3+}- co-doped nanomaterials have been reported: $BiPO_4$ chromaticity coordinates of (0.318, 0.356) [9], $GdPO_4$ (0.328, 0.327) [11], YVO_4 (0.323, 0.325) [13] and SiO_2-coated and doped $GdVO_4$ with CIE coordinates located at the center of the white area [14].

4. Conclusions

We have demonstrated that the concentrations of dopant ions in $Ho^{3+}/Er^{3+}/Tm^{3+}$- doped and Yb^{3+}- co-doped $GdVO_4$ nanocrystalline powders can be optimized to enable white UC emission from material under NIR irradiation at 982 nm. This was achieved because Ho^{3+} ions in $GdVO_4$ provide the red UC emission, contrary to the green UC emission observed in the majority of other host materials. Then, the white light UC was obtained from combinations of three color emissions in four samples in $GdVO_4$ with the following concentrations of dopant ions: 10 mol%Tm,2 mol% Er,0.5 mol%Ho,40 mol%Yb (two samples: annealed at 800 °C and 1000 °C) that emit light with the chromaticity coordinates of (0.326, 0.339) and (0.346, 0.343) 10 mol%Tm,2 mol%Er,1 mol% Ho,40 mol%Yb (two samples: annealed at 800 °C and 1000 °C) with the chromaticity coordinates of (0.323, 0.327) and (0.342, 0.340). The color of the UC emission can be tuned between red (0.504, 0.369), green (0.282, 0.577) and blue (0.142, 0.125) by varying doping composition and concentration of lanthanide ions in $GdVO_4$ nanoparticles. Further investigations will analyze differences in UC efficiency between the mixture of single doped powders and the multi-doped samples.

References

[1] Yu Z, Yang Q, Xu CA, Liu Y. Upconversion white-light emitting of Tm^{3+} and Er^{3+} codoped oxyfluoride and its achieving mechanism. Mater. Res Bull 2009;44:1576–80.
[2] Zhou B, Tao L, Tsang YH, Jin W. Core−shell nanoarchitecture: a strategy to significantly enhance white-light upconversion of lanthanide-doped nano-particles. J Mater Chem C 2013;1:4313–8.
[3] Rozhnova YA, Luginina AA, Voronov VV, Ermakov RP, Kuznetsov SV, Ryabova AV, et al. White light luminophores based on $Yb^{3+}/Er^{3+}/Tm^{3+}$-coactivated strontium fluoride powders. Mater Chem Phys 2014;148:201–7.
[4] Wang F, Liu X. Multicolor tuning of lanthanide-doped nanoparticles by single wavelength excitation. Acc Chem Res 2014;47:1378–85.
[5] Wang F, Liu X. Recent advances in the chemistry of lanthanide-doped upconversion nanocrystals. Chem Soc Rev 2009;38:976–89.
[6] Haase M, Schäfer H. Upconverting nanoparticles. Angew Chem Int Ed 2011;50:5808–29.
[7] Chen J, Zhao JX. Upconversion nanomaterials: synthesis, mechanism, and applications in sensing. Sensors 2012;12:2414–35.
[8] Han X, Castellano-Hernández E, Hernández-Rueda J, Solís J, Zaldo C. White and full color upconversion film-on-glass displays driven by a single 978 nm laser. Opt Express 2014;22:24111–6.
[9] Wang Z, Feng J, Pang M, Pan S, Zhang H. Multicolor and bright white upconversion luminescence from rice-shaped lanthanide doped $BiPO_4$ sub-micron particles. Dalton Trans 2013;42:12101–8.
[10] Barrera EW, Pujol MC, Carvajal JJ, Mateos X, Sole R, Massons J, et al. White light upconversion in Yb-sensitized (Tm, Ho)-doped $KLu(WO4)_2$ nanocrystals: the effect of Eu incorporation. Phys Chem Chem Phys 2014;16:1679–86.
[11] Fu Z, Sheng T, Wu Z, Yu Y, Cui T. A novel and tunable upconversion lumi-nescent material $GdPO_4$: Yb^{3+}, Ln^{3+} (Ln = Er, Tm, Ho). Mater. Res Bull 2014;56:138–42.
[12] Xu Y, Wang Y, Shi L, Xing L, Tan X. Bright white upconversion luminescence in $Ho^{3+}/Yb^{3+}/Tm^{3+}$ triple doped $CaWO_4$ polycrystals. Opt Laser Technol 2013;54:50–2.
[13] Sun J, Yhu J, Liu X, Du H. Bright white up-conversion emission from $Er^{3+}/Ho^{3+}/Tm^{3+}/Yb^{3+}$ co-doped YVO_4 phosphors. Mater Res Bull 2013;48:2175–9.
[14] Calderón-Villajos R, Zaldo C, Cascales C. Enhanced upconversion multicolor and white light luminescence in SiO_2-coated lanthanide-doped $GdVO_4$. Nanotechnology 2012;23:10. 505205.
[15] Mahalingam V, Naccache R, Vetrone F, Capobianco JA. Enhancing upconverted white light in $Tm^{3+}/Yb^{3+}/Ho^{3+}$-doped $GdVO_4$ nanocrystals via incorporation of Li^+ ions. Opt Express 2012;20:111–9.
[16] Xia Z, Zhou W, Du H, Sun J. Synthesis and spectral analysis of $Yb^{3+}/Tm^{3+}/Ho^{3+}$-doped $Na_{0.5}Gd_{0.5}WO_4$ phosphor to achieve white upconversion lumi-nescence. Mater Res Bull 2010;45:1199–202.
[17] Jovanović DJ, Antić Z, Krsmanović RM, Mitrić M, Đordević V, Bártová B, et al. Annealing effects on the microstructure and photoluminescence of Eu^{3+}-doped $GdVO_4$ powders. Opt Mater 2013;35:1797–804.
[18] Gao W, Wang R, Han Q, Dong J, Yan L, Zheng H. Tuning red upconversion emission in single $LiYF_4$:Yb^{3+}/Ho^{3+} microparticle. J Phys Chem C 2015;119: 2349–55.
[19] Chung JH, Ryu JH, Lee SY, Lee JH, Choi BG, Shim KB. Yellow lighting upcon-version from Yb^{3+}/Ho^{3+} co-doped $CaMoO_4$. Mater Res Bull 2012;47:1991–5.
[20] Gavrilović TV, Jovanović DJ, Trandafilović LV, Dramićanin MD. Effects of Ho^{3+} and Yb^{3+} doping concentrations and Li^+ co-doping on the luminescence of $GdVO_4$ powders. Opt Mater 2015;45:76–81.
[21] Li X, Zhu J, Man Z, Ao Y, Chen H. Investigation on the structure and upcon-version fluorescence of Yb^{3+}/Ho^{3+} co-doped fluorapatite crystals for potential biomedical applications. Sci Rep 2014;4:4446.
[22] Gavrilović TV, Jovanović DJ, Lojpur V, Dramićanin MD. Multifunctional Eu^{3+}- and Er^{3+}/Yb^{3+}-doped $GdVO_4$ nanoparticles synthesized by reverse micelle method. Sci Rep 2014;4:4209.
[23] Zhang Y, Li X, Kang X, Hou Z, Lin J. Morphology control and multicolor upconversion luminescence of GdOF: $Yb^{3+}/Er^{3+},Tm^{3+},Ho^{3+}$ nano/sub-microcrystals. Phys Chem Chem Phys 2014;16:10779–87.